Front. Struct. Civ. Eng. 2021, 15(1): 109–123
https://doi.org/10.1007/s11709-021-0693-0

RESEARCH ARTICLE

# Experimental study on compaction-induced anisotropic mechanical property of rockfill material

**Xiangtao ZHANG, Yizhao GAO, Yuan WANG, Yu-zhen YU*, Xun SUN**

*State Key Laboratory of Hydroscience and Engineering, Department of Hydraulic Engineering, Tsinghua University, Beijing 100084, China*

*Corresponding author. E-mail: yuyuzhen@mail.tsinghua.edu.cn*



**ABSTRACT** The anisotropy of rockfill materials has a significant influence on the performance of engineering structures. However, relevant research data are very limited, because of the difficulty with preparing specimens with different inclination angles using traditional methods. Furthermore, the anisotropy test of rockfill materials is complex and complicated, especially for triaxial tests, in which the major principal stress plane intersects with the compaction plane at different angles. In this study, the geometric characteristics of a typical particle fraction consisting of a specific rockfill material were statistically investigated, and the distribution characteristics of particle orientation in specimens prepared via different compaction methods were examined. For high-density rockfill materials, a set of specimen preparation devices for inclined compaction planes was developed, and a series of conventional triaxial compression tests with different principal stress direction angles were conducted. The results reveal that the principal stress direction angle has a significant effect on the modulus, shear strength, and dilatancy of the compacted rockfill materials. Analysis of the relationship between the principal stress direction angles, change in the stress state, and change in the corresponding dominant shear plane shows that the angle between the compacted surface and dominant shear plane is closely related to interlocking resistance associated with the particle orientation. In addition, different principal stress direction angles can change the extent of the particle interlocking effect, causing the specimen to exhibit different degrees of anisotropy.

**KEYWORDS** rockfill, inclination of specimen preparation, anisotropy, mechanical property, mechanism

## 1 Introduction

China is rich in rockfill materials, which have many excellent engineering properties, such as high compacted density, high shear strength, good permeability, and favorable liquefaction resistance [1], and have therefore been widely used in high-fill, high-earth-rockfill dams and railway foundations, among many other engineering applications. This paper focuses on research on compacted rockfill in earth-rockfill dams. Both the concrete-face rockfill dam and core-wall rockfill dam are two common dam types in China, occupying an increasingly large proportion of high dams built or under construction in the country. As the main filling materials of core-wall rockfill dams, rockfill materials usually account for more than two-thirds of the entire dam body, whereas in concrete-face rockfill dams, the proportion of rockfill materials can reach approximately 99% of the entire dam body. In actual dam construction processes, strong compaction causes the rockfill particles to form distribution features with long axes favorable along the horizontal direction, which enable the mechanical properties of the rockfill to be anisotropic. (An important point to note is that the anisotropic formation mechanism of rockfill differs from that of rocks in the earth's crust [2].) Therefore, a rockfill dam is usually characterized by high density and transverse isotropy as a result of strong horizontal-layered compaction during the construction process.

A rockfill dam is characterized by a complex stress state during the construction and water impounding processes. The major principal stress plane is not necessarily consistent with the compaction plane. The major principal stress plane in a rockfill dam is almost identical to the horizontal compaction plane during the filling period of the

*Article history: Received Dec 20, 2019; Accepted Mar 22, 2020*

dam, but changes significantly during the impounding period. For a concrete-face rockfill dam, the upstream water pressure acts vertically on the inclined concrete face during the impounding period, which enables the major principal stress plane in the rockfill behind the face to deviate from the compaction plane. For a core-wall rockfill dam, the upstream rockfill is subjected to upward buoyancy during the impounding period, allowing more horizontal displacement to occur because of the water pressure acting on the core wall. Consequently, the direction of the major principal stress in both the upstream and downstream rockfills may vary significantly. Furthermore, once the constraint effect of the river valley is considered, changes in the major principal stress direction become more complicated.

Both theory and practice have demonstrated that the anisotropy of rockfill materials has a significant influence on the mechanical behavior of rockfill dams [1]. For example, when the mechanical behavior of a high rockfill dam is analyzed using a numerical method such as the finite element method (FEM), the calculated horizontal displacement and its relative relationship with the vertical displacement are far from the measured results. One of the important reasons for this deviation is that the anisotropy of the rockfill is not sufficiently considered in the constitutive model. Therefore, the anisotropy of rockfill materials due to construction compaction has attracted much attention from engineers and academic communities in recent years. In particular, with the construction of increasingly higher rockfill dams, it has become more urgent to perform research on the anisotropic properties of rockfill.

Researchers have been studying this topic from a variety of perspectives. For example, Yang et al. [3] and Jia [4] conducted a variety of complex stress path tests to investigate the mechanical properties of rockfill under complex stress conditions and their effects on rockfill dams. With regard to the application of constitutive models to complex stress paths, many test results have shown that most existing constitutive models can be used to effectively simulate properties along stress paths under the condition of strain control or in a conventional triaxial state [5–8]. However, existing constitutive models are very difficult to use for accurately simulating mechanical properties under some of the more complex stress paths.

Thus far, few experimental studies have been conducted on the anisotropic mechanical properties of rockfill materials. On the other hand, available research data on the anisotropic properties of soil have been focused mainly on clay and sand [5,6,9–11]. For example, Duncan and Seed [12] determined that anisotropy and stress reorientation may cause the undrained strength of clay to change with the direction of the failure plane. To study the anisotropy of sand, a variety of tests have been conducted using different types of equipment, such as direct shear apparatus [13,14], plane strain tests [15], true triaxial apparatus [16–21], and hollow cylinder torsional shear apparatus [22–29]. For example, Oda et al. [15] investigated the anisotropic properties of sand using plane strain tests, in which dense samples of Toyoura sand were prepared in a tilting mold to provide different directions of sample deposition with respect to the principal stress axes. Chaudhary et al. [30] used a hollow-cylinder torsional shear device to study the influence of initial fabric and shear direction on the cyclic deformation characteristics, such as the stress–strain response, shear modulus, and damping ratio, of medium-density Toyoura sand. Shi [6] used a true triaxial apparatus to conduct single-direction loading tests on coarse-grained soil in different principal stress directions and studied the stress-induced anisotropy of coarse-grained soil. Yang [28] employed different methods with an image-analysis-based technique and an appropriate mathematical approach in the preparation of sand specimens in the laboratory, and quantitatively measured and compared the fabrics of the sand specimens at a microscopic level. They observed that the specimen prepared via dry deposition had a more anisotropic microstructure than that of the specimen prepared via moist tamping. Yang et al. [31] conducted a series of triaxial and torsional shear tests on Toyoura sand to explore the relationship between soil response and fabric anisotropy. Based on their results, the differences in the undrained stress–strain response among the differently prepared specimens were attributed to fabric anisotropy. Meanwhile, Suwal and Kuwano [32] measured the Young's modulus and Poisson's ratio in all three directions of coarse-grained soil specimens by applying elastic waves using a disc-type sensor, and compared and analyzed the vertical and lateral differences of coarse-grained soil.

Computational simulation, which is the third primary methodology for solving a wide range of scientific and engineering problems [33–36], can applied to the study of the anisotropy behavior of coarse-grained soils. Several numerical experiments investigating the properties of granular materials have already been conducted. For instance, Zhang [37] used the discrete element method to conduct numerical simulations of true triaxial tests on granular materials under different shear modes and stress paths, and investigated the influence of intermediate principal stress on the anisotropy and anisotropy strength characteristics of granular materials under complex stress states. Chu et al. [38] proposed an elastoplastic model suitable for coarse-grained soil based on initial results of anisotropy research on fine-grained soil, which may reflect the anisotropy state of coarse-grained soil. Zhang et al. [39] modified a double-yield-surface elastoplastic constitutive model via stress transformation and introduction of a new stress ratio parameter according to experimental data, such that the anisotropy of coarse-grained soil is accounted for in the study.

With regard to rockfill materials, on the other hand, whereas the aforementioned computational simulation

methods may be extended to describe some anisotropic mechanical properties of rockfill materials, little direct experimental evidence exists to verify whether this approach is reasonable.

Oda and Nakayama [40] listed the following three main sources of inherent anisotropy in granular materials: 1) anisotropic distribution of contact normals, representing the relationship among particles; 2) distribution direction of the long axis of pores; and 3) distribution direction of the long axis of non-spherical particles. Through a biaxial compression test of a two-dimensional bar assembly, Oda et al. [41] also observed that the inherent anisotropy caused by 1) and 2) tended to disappear completely at the early stage of inelastic deformation, whereas the inherent anisotropy caused by 3) remained into the final stage of deformation. Therefore, the anisotropy, which significantly influences the mechanical properties of compacted rockfill, is caused mainly by the orientation of the particles. In addition, in the construction process, the degrees of orientation of rockfill particles due to different compaction intensities are different, and thus the degrees of influence of the anisotropy of the materials on their engineering characteristics are also different. This relationship indicates that the anisotropy of rockfill materials can have a significant influence on the engineering performance of high earth-rockfill dams, although relevant research work will be necessary to verify this hypothesis. However, thus far, little has been achieved on the most basic research data because of the difficulties with preparing specimens with different inclination angles using traditional methods. Furthermore, anisotropy tests on rockfill materials, especially triaxial tests with different angles between the principal stress plane and the compaction plane, tend to be complex and complicated.

In laboratory triaxial tests to investigate the anisotropic properties of soil, the traditional method of specimen preparation is to deposit or to compact soil in a large container, and then to cut the required specimen at different inclination angles. In the case of sand, the specimen should be frozen or sprayed onto a tilting mold before cutting. The disadvantages of using these methods are as follows: the structure of granular materials may be destroyed during cutting, and a specimen containing large particles cannot be cut in a way that reflects the material characteristics. These limitations imply that it is not feasible to use traditional methods, such as freezing, cutting, or tilting mold cutting, to prepare specimens of rockfill materials, which are characterized by large particle sizes and no cohesion, at different inclination angles. Moreover, whereas torsion shear tests using a hollow cylinder can also be applied to study the mechanical properties of sand or clay specimens when the principal stress plane intersects with the compaction plane at different angles, no such large hollow-cylinder apparatus exists thus far for large-particle-size materials such as rockfill materials.

Based on the aforementioned considerations, the geometric characteristics of the typical particle fraction of a certain rockfill material were first analyzed in this study. The distribution features of the particle arrangement directions in simulated specimens with different compaction intensities were then investigated. To examine the high-density rockfill material, a set of specimen preparation devices, which can enable the compaction plane and bottom plane of the rockfill specimen to have different inclination angles, was manufactured. A series of conventional triaxial compression tests, in which the major principal stress plane intersects with the specimen compaction plane at different angles, were then conducted. Based on relevant test results, the influence of the major principal stress direction angle, i.e., the angle between the major principal stress plane and the compaction plane, on the mechanical properties of the compacted rockfill material was investigated, and the formation mechanism of the anisotropic shear strength of the compacted rockfill material was analyzed.

## 2 Statistical analysis of geometric characteristics of rockfill particles and simulated specimen

The rockfill materials used in this research were obtained from the main rockfill material ground of a planned 300-m-high earth-rockfill dam in south-west China, with a maximum particle size of 600 mm in the original gradation. Scaling the original gradation was necessary because of the limitation of the test equipment, and thus a maximum particle size of 40 mm was imposed on the test specimen.

### 2.1 Particle shape features of tested rockfill material

In most projects, rockfill materials are obtained via mechanical crushing after the rock mass is blasted. The resulting rockfill particles are irregular and angular in shape, with axial length ratios greater than 1 and with many angles. Figure 1 shows photos of typical large- and medium-sized particles in the specimen.

To quantitatively analyze the shape features of the rockfill particles, three axial lengths were measured. As shown in Fig. 1, the axial lengths of irregular particles in the three directions are denoted and defined as follows: maximum axial length $d_1$, which is the longest side length of the maximum particle projection plane; medium axial length $d_2$, which is the shortest side length of the maximum particle projection plane; and minimum axial length $d_3$, which is the shortest side length of the minimum particle projection plane.

The rockfill material used in the test was composed of a variety of particle fractions with different particle sizes mixed together according to a predetermined gradation curve. Because the coarse particle fractions definitely

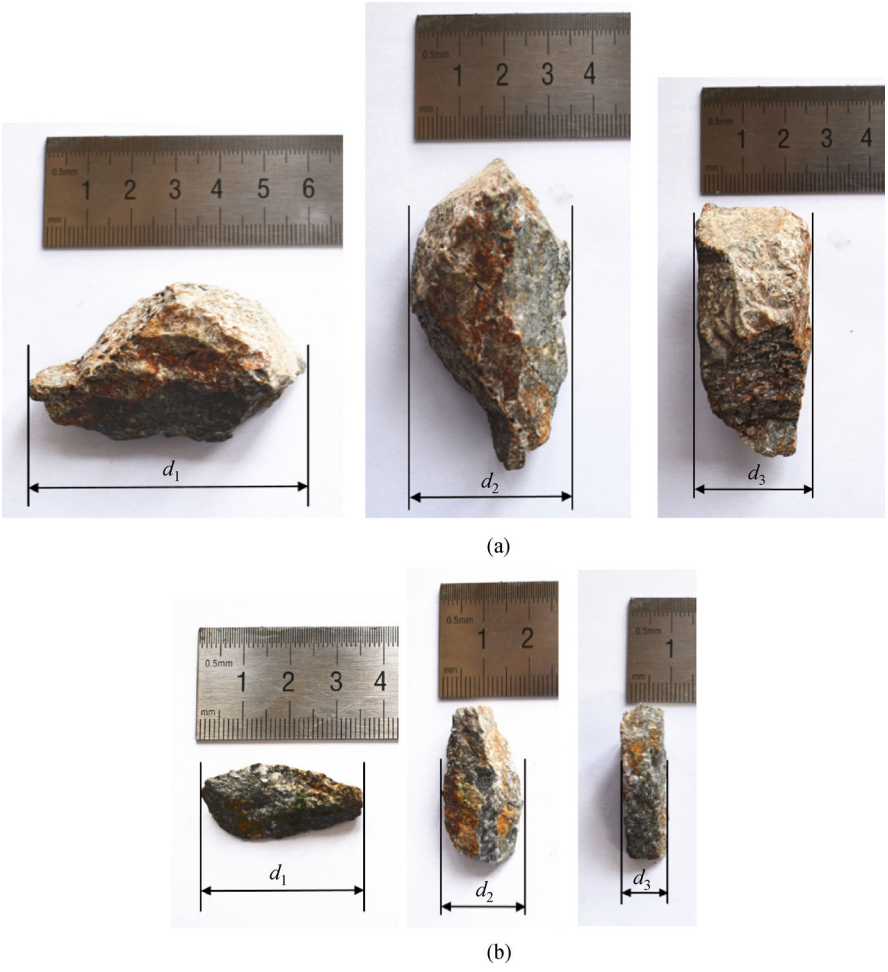


**Fig. 1** Photos of two typical particles of the rockfill: (a) a large-size particle; (b) a medium-size particle.

influence the mechanical properties of rockfill and for the convenience of measurement, only the characteristic axes of two groups with relatively large particle sizes were counted. Each of these groups had 50 particles. Figure 2 shows the probability densities of the characteristic axial length ratios of the two groups of rockfill particles. As can be seen from this figure, for the large-sized particle fraction, $d_1/d_3$ ranges from 1 to 6, with an average value of 2.59, whereas $d_2/d_3$ ranges from 1 to 4, with an average value of 1.72. For the medium-sized particles, on the other hand, $d_1/d_3$ ranges from 1 to 10, with an average value of 3.36, whereas $d_2/d_3$ ranges from 1 to 8, with an average value of 1.83. Through analysis of the ratios of the three characteristic axes, the axial lengths in the three directions of both particle fractions are observed to be clearly different, with the maximum projected area being approximately 4 to 6 times the minimum.

### 2.2 Distribution features of particle direction of simulated rockfill specimen

Different compaction intensities or specimen preparation methods lead to different orientations of rockfill particles. To study the influence of anisotropy on the mechanical properties of rockfill materials, quantitative analysis of this factor is necessary. The specimens subjected to the triaxial test have a large range of various particle sizes, and thus the following two problems exist in the process of obtaining statistics on the arrangement directions of all particle fractions: massive workload, and inconvenience of extracting the main information. To highlight the main factors, to improve the observation accuracy, and to quantitatively study the influence of different specimen preparation densities on the anisotropy of the rockfill material, only the large-sized particle fraction (particle size range: 20 to 40 mm) was used in this investigation. Three specimens were prepared in a 200 mm × 200 mm × 400 mm stainless-steel box mold using different methods. In the first method, the specimen was prepared via free fall of rockfill particles from a height of 40 cm above the top of a specimen without compaction, resulting in a specimen of density 1.54 g/cm$^3$, which was called the low-density specimen. In the second method, the specimen was prepared layer by layer with a moderate level of compaction, resulting in a specimen of density 1.73 g/cm$^3$, which was called the medium-density specimen. In the

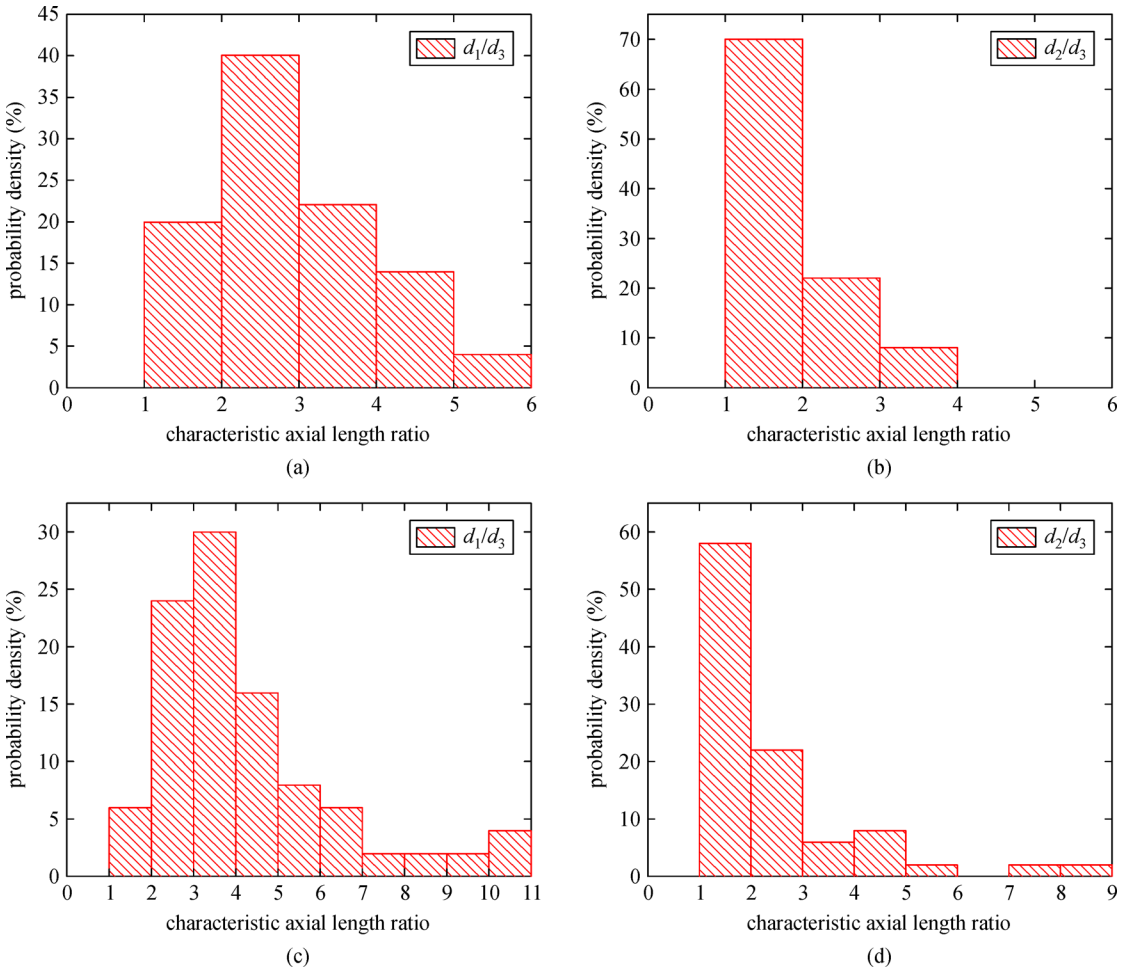


**Fig. 2** Probability density of characteristic axial length ratios of rockfill particles: (a) statistical diagram of characteristic axial length ratio $d_1/d_3$ for large-size particle groups; (b) statistical diagram of characteristic axial length ratio $d_2/d_3$ for large-size particle groups; (c) statistical diagram of characteristic axial length ratio $d_2/d_3$ for medium-size particle groups; (d) statistical diagram of characteristic axial length ratio $d_2/d_3$ for medium-size particle groups.

third method, the specimen was prepared layer by layer with a relatively strong degree of compaction, resulting in a specimen of density 1.82 g/cm$^3$, which was called the high-density specimen. When the mold was fully filled with rockfill, the upper cover plate was installed. One of the side plates was then replaced with a plexiglass plate, the observed rockfill particles were drawn in the long-axis direction, and the inclination angle was measured and counted.

Figure 3 shows a schematic diagram of the particle inclination angle, which is defined as the angle between the long axis of the particle and the horizontal plane. The upper right inclination is positive, and the lower right inclination is negative, with a variation range of –90° to 90°. Because only one plane is observed, the long axis of particles on this plane may be the long axis or the middle axis under three-dimensional conditions, but the results do not affect the orientation distribution analysis of the particles. Figure 4 shows the orientation distributions of

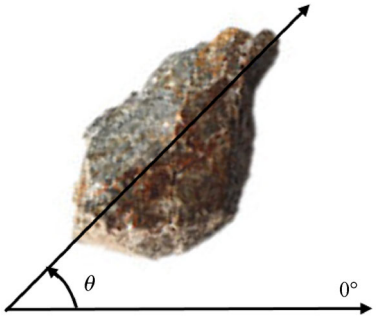


**Fig. 3** Schematic diagram of particle inclination angle.

the particles at three different densities. In this figure, black lines are drawn on each observable particle along the long axis to indicate their inclination directions. The distributions of the particle inclination angle under three different density conditions were statistically analyzed, and the

(a)

(b)

(c)

**Fig. 4** Distribution of particle orientations: (a) low-density specimen; (b) medium-density specimen; (c) high-density specimen.

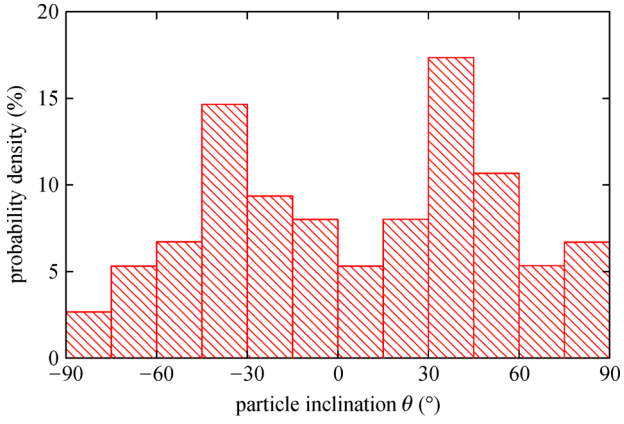


(a)

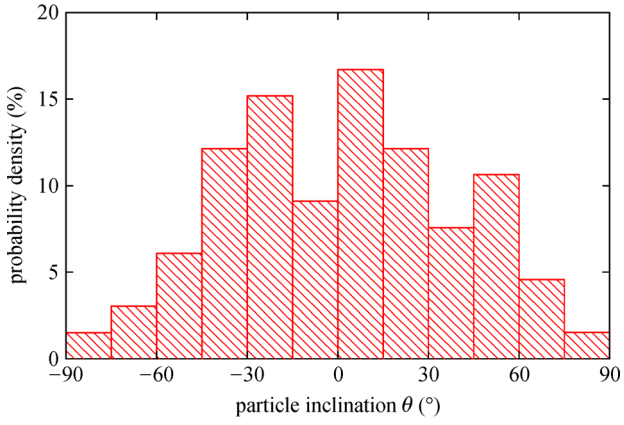


(b)

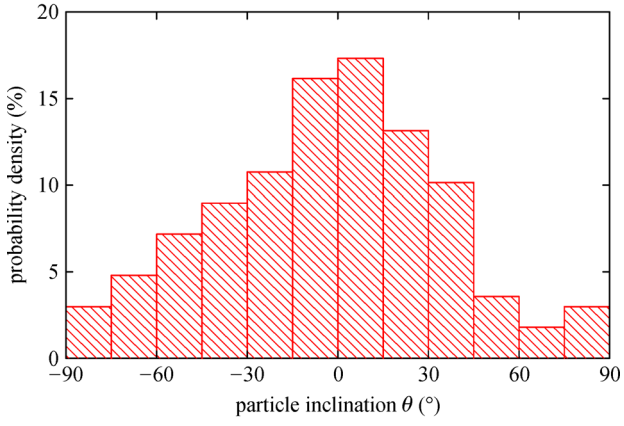


(c)

**Fig. 5** Probability distribution of particle inclination: (a) low-density specimen; (b) medium-density specimen; (c) high-density specimen.

corresponding results are visualized in Fig. 5. The numbers of particles counted for the orientation characteristic in the three specimens were 95, 109, and 120, respectively.

As shown in Fig. 5(a), the particle inclination angle distribution histogram of the low-density specimen is characterized by two peaks in the probability distribution graph, at approximately ±(30–45)°. There are also two peaks in the probability distribution histogram for the particle inclination angle of the medium-density specimen, at approximately +(0–15)° and –(15–30)°, as shown in Fig. 5(b). On the other hand, the probability distribution histogram for the particle inclination angle of the high-density specimen, shown in Fig. 5(c), has only one peak, which is near 0° and is relatively concentrated. The proportion for the particle inclination angle between ±15° is approximately 35%, and that between ±30° is approximately 60%. It can be inferred that, with the increase in compaction density, the particle inclination angle associated with the peak of the probability distribution histogram approaches zero, implying that the orienta-

tion of particles in the rockfill specimen tends toward the horizontal direction. In other words, the compaction effect of specimen preparation significantly enhances the horizontal orientation of the particles. In the construction process of a rockfill dam, rockfill materials are strongly compacted to a very high density. When a laboratory triaxial test is conducted, layer-by-layer compaction should be performed during the specimen preparation process to ensure that the specimen can reach the required high density. In addition, because the particle size distribution can have a wide range, the horizontal orientation tendency of the particles should be more obvious. The predominant arrangement direction of the particles is considered to be parallel to the compaction surface; namely, the compaction-surface-parallel direction can be regarded as the representative direction of the particle arrangement.

## 3 Triaxial test for different angles of major principal stress direction

### 3.1 Basic test conditions and test scheme

The maximum particle size of the main rockfill dam was 600 mm, and the parent rock was mainly dacite. The cubic specimen size for the triaxial test was 200 mm × 200 mm × 400 mm. The minimum ratio of the diameter $D$ of the specimen to the adopted maximum particle size $d_{max}$ in the triaxial test was 5:1 (for the ASTM standard), and thus the maximum allowable particle size of 40 mm in the test was able to satisfy this criterion. The particle gradation of the specimen was obtained via a mixed method of similar gradation and equal substitution methods. The dry density of the specimen of the tested rockfill material was $\rho_d = 2.05$ g/cm$^3$. Figure 6 shows the grading curves of the specimen and prototype rockfill.

A series of conventional triaxial tests, complex stress path tests, and true triaxial tests were conducted on rockfill materials at an earlier stage of this study [42]. On the other hand, the objective of this study is to investigate the influence of the major principal stress direction angle on the anisotropic mechanical properties of the rockfill material, and thus only one confining pressure was used, namely $\sigma_3$ = 400 kPa. For the angle between the major principal stress plane and the compaction plane, namely the major principal stress direction angle, $\delta$ = 0°, 15°, 30°, 45°, 60°, 75°, and 90° were selected for the preparation of corresponding specimens. THU-SDTTA [6], a large-scale static and dynamic true triaxial apparatus at Tsinghua University, was used for conducting a series of conventional triaxial drainage shear tests. After consolidation under a confining pressure of 400 kPa, the porosity of the specimen was approximately 0.257. The difficult part of the test was to prepare a rockfill specimen with the bottom intersecting with the compaction plane at the specified angle.

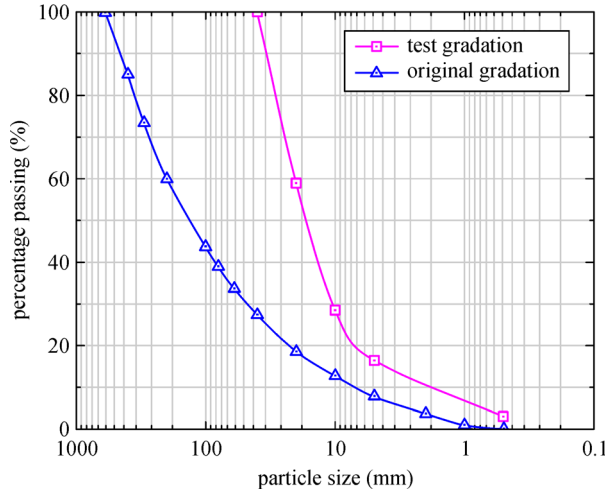


**Fig. 6** Grading curves of the specimen and prototype rockfill.

### 3.2 Specimen preparation device

There are three main difficulties in preparing a high-density specimen of rockfill materials. First, to achieve high density, layer-by-layer compaction, careful control should be implemented. Second, the apparent cohesion of rockfill materials is basically zero, and thus the self-standing capacity of the rockfill specimens is very poor. Because it is usually difficult to maintain the specimen shape during preparation and installation, special measures should be enforced to avoid specimen disturbance as much as possible. Third, with regard to the test schemes for different major stress direction angles, because of the large particle size and poor self-standing capacity of rockfill materials, it is impossible to use traditional cutting methods for specimen preparation or to directly conduct a hollow-cylinder torsion shear test, and thus, a new specimen preparation method will have to be developed.

To overcome the aforementioned difficulties in the process of rockfill specimen preparation, we developed a set of specimen preparation devices with arbitrary inclination angles of the compaction plane, specifically for coarse-granular geotechnical materials such as rockfill materials. Figure 7(a) illustrates the overall structure of the device. The specimen preparation device includes mainly a mold box that can be rotated at the bottom side, a strut that can stretch out and draw back freely, and a bracket connected to one end of the mold box by a rotating shaft. The mold box is a cuboid with the top and its adjacent side open, which can be sealed by block-inserted baffles. The bracket consists of a rotating shaft that can fix the mold box and a supporting steel frame at the bottom. The strut connects the base with a joint, and the frame is fixed onto the base. An additional protractor is used to measure the inclination angle of the mold box.

Before specimen preparation, the retraction amount of the strut was adjusted to satisfy the required angle between

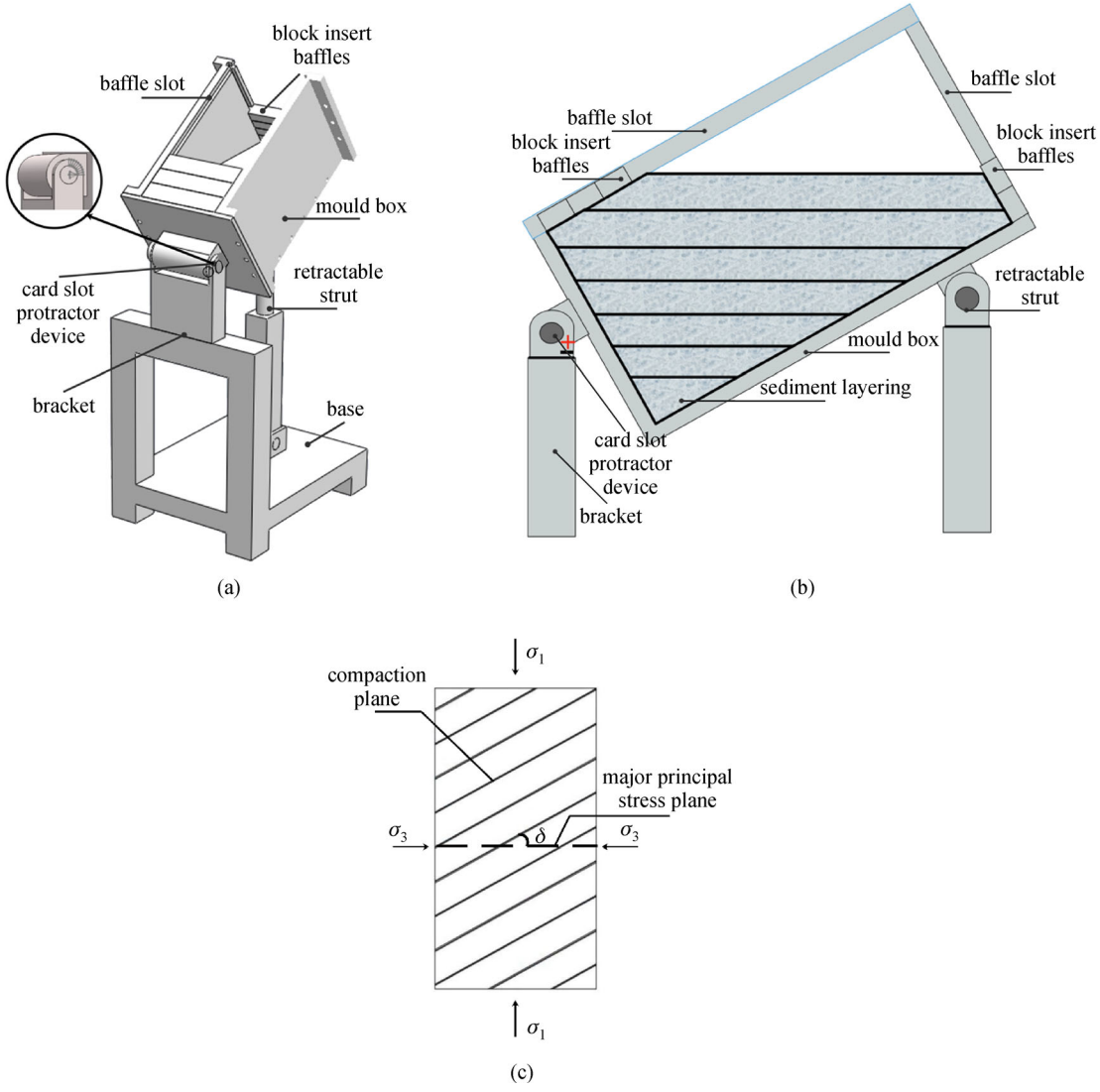


**Fig. 7** Specimen preparation device for rockfill with arbitrary inclination angle of compaction plane: (a) overall diagram; (b) schematic diagram of layer-wise specimen; (c) relationship between compaction plane and principal stress plane.

the compaction plane and loading direction in the test. The mold box was then adjusted to the corresponding position and fixed. Finally, all the baffles were removed, and the mold box was opened on both sides. Because of the rich edges and corners of rockfill materials, it is necessary to line the inside of the mold box with a rubber film, which has been cut and formed with strong adhesive in advance, to wrap the specimen. The two open sides of the rubber film were not spliced at this stage to leave space for the compaction of rockfill materials. For each layer, a certain amount of rockfill, which was pre-weighed according to the target density of the specimen, was evenly sprinkled over the mold box, and compaction was performed layer by layer (as shown in Fig. 7(b)) using compaction hammers of two different sizes. Because the bottom areas of the compaction hammers were much less than that of the upper surface of the specimen, the impact of this compaction on the lower layers was small during the compaction process. When the material reached the top of the open sides, the blocked baffles were gradually inserted along the slots. As the height of the inserted baffles increased, the rubber film on the opening sides was spliced with super glue in time to maintain the height of the rubber film on the open sides to be the same as that of the inserted baffle. During the compaction process, five points were selected for the measurement of the vertical distance from the top of the mold for each layer after compaction, to strictly control the specimen density according to the layer thickness. As the compaction process proceeded, each baffle was inserted gradually to restrain the scattered particles that had been filled until the end of the compaction operation. The last baffle was inserted to

complete the specimen preparation.

Whole freezing was necessary to reduce the disturbance of the specimen due to installation. Therefore, during the preparation process, an appropriate amount of water, such that the specimen can be frozen with a certain strength and little frost heave, was sprinkled onto the surface of the specimen.

The prepared specimen, together with the mold, was placed into a freezer. After the specimen was frozen evenly, it was removed, inserted into latex film, and then installed into the testing apparatus.

When the triaxial test was to be conducted, the specimen was placed onto the pedestal of the chamber, with the minor sides of the specimen at the top and bottom, such that the long-side direction of the specimen was identical to the vertical direction, namely the direction of the major principal stress. The relationship between the compaction plane and major stress is shown in Fig. 7(c).

### 3.3 Results of triaxial tests

A group of seven tests was conducted according to the aforementioned schemes and methods, and the test results are shown in Fig. 8. Figure 8(a) shows the deviatoric stress versus the axial strain curves of the conventional consolidated drained (CD) triaxial tests with a confining pressure of $\sigma_3$ = 400 kPa. The seven curves correspond to the major principal stress direction angles $\delta$ = 0°, 15°, 30°, 45°, 60°, 75°, and 90°. Meanwhile, Fig. 8(b) shows the corresponding volumetric strain versus axial strain curves.

### 3.4 Analysis of test results

As shown in Fig. 8(a), under a confining pressure of

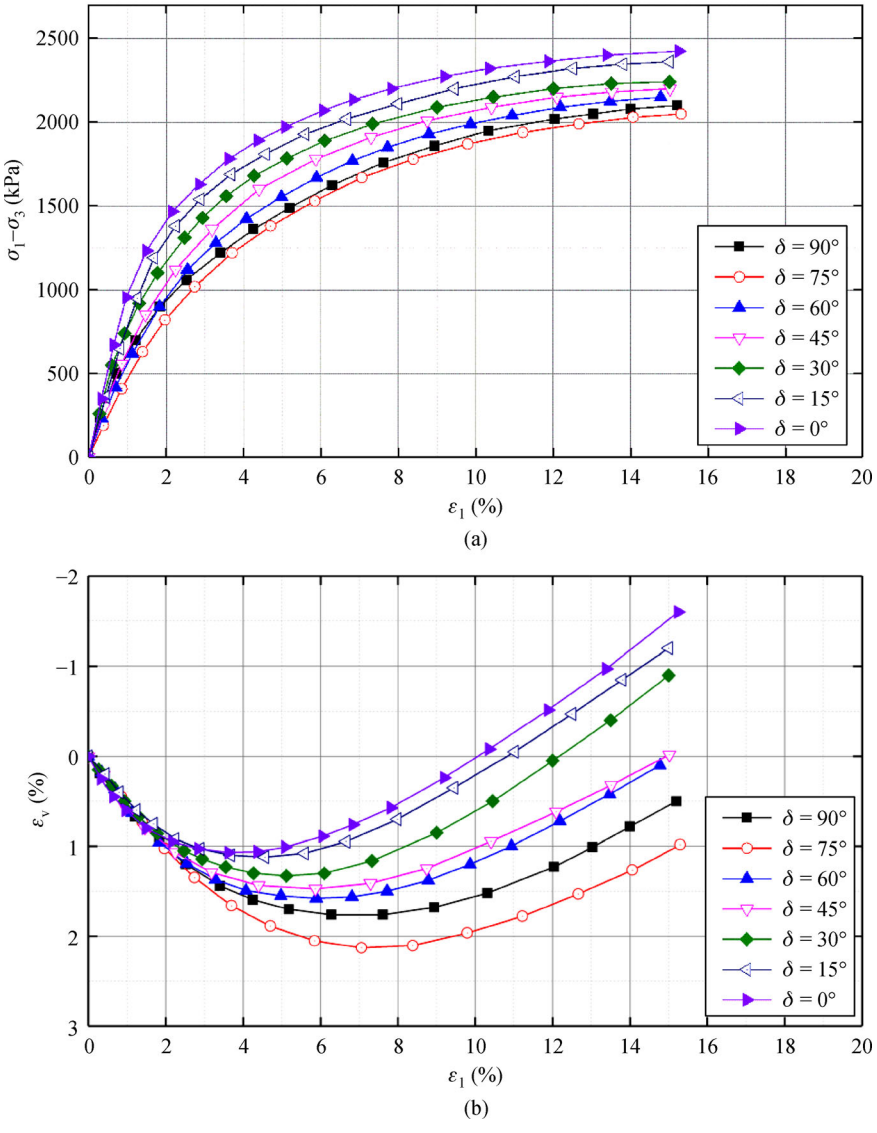


**Fig. 8** Conventional CD triaxial test results with various major principal stress direction angles: (a) stress-strain relationship curves; (b) volumetric strain versus axial strain curves.

400 kPa, the deviatoric stress–axial strain behaviors for the different major principal stress direction angles were similar, and exhibit characteristics of strong nonlinearity. At the initial stage, the deviatoric stress clearly increased with the increase in axial strain. At the end of the test, when the axial strain reached $\varepsilon_1$ = 15%, the deviatoric stress increased slowly, and a peak value did not appear. In this study, it was assumed that the stress state at $\varepsilon_1$ = 15% corresponds to the strength of the specimen. When $\delta$ changed from 0° to 75°, the strength of the specimen decreased with the increase in $\delta$, and then increased slightly at $\delta$ = 90°. This result indicates that, in this study, the strength of the specimen in the conventional CD triaxial test did not increase monotonously with the increase in the major principal stress direction angle, and that the peak strength of the specimen reached its lowest value at $\delta$ = 75°. This tendency is consistent with the characteristics of sand determined previously by many other researchers [13,43–45].

In similar tests on sands for different directions of sample deposition with respect to the principal stress axes, when the axial strain reached a certain value, such as 6% in the tests by Oda et al. [15], the stress–strain curves tended to be consistent. However, for the rockfill materials examined in this study, when the axial strain of the specimens with different principal stress direction angles reaches 15%, the stress–strain curves are still clearly separated from each other. This may be a result of the strong interlocking effect between the particles of the rockfill material, which is not easy to adjust during loading.

As shown in Fig. 8(b), at the early stage of shearing, the specimen contracted with an increase in the axial strain, but the slope of the volumetric strain decreased gradually. After the axial strain reached a certain level, the volumetric strain changed from contraction to expansion, and the apparent dilatancy was still obvious when $\varepsilon_1$ reached 15%. When $\delta$ varied from 0° to 75°, the dilatancy of the specimen became increasingly weaker. However, the dilatancy of the specimen increased slightly at $\delta$ = 90°.

Figure 9 shows the secant modulus of the specimens at the initial stage of the conventional CD triaxial tests for different major principal stress direction angles. Because of the relatively large test error at the initial stage of loading, the secant modulus of the specimens between $\varepsilon_1$ = 0 and $\varepsilon_1$ = 2% was used for comparison. According to this figure, the initial secant modulus $E_s$ at $\delta$ = 0° was 70.75 MPa, which then gradually decreased with the increase in $\delta$, and reached a minimum value of 42.5 MPa at $\delta$ = 75°. However, the initial secant modulus of the specimens increased to some extent at $\delta$ = 90°.

Figure 10 visualizes the strength parameters $M$ and $\varphi$ of the specimens in the conventional CD triaxial tests with different major principal stress direction angles. The strength parameters $M$ and $\varphi$ are the ratio of the generalized shear stress to the mean stress and the converted internal friction angle of the specimen at $\varepsilon_1$ = 15%, respectively. The values of these strength parameters decreased gradually until they reached their minimum values at $\delta$ = 75°. However, the values increased slightly at $\delta$ = 90°.

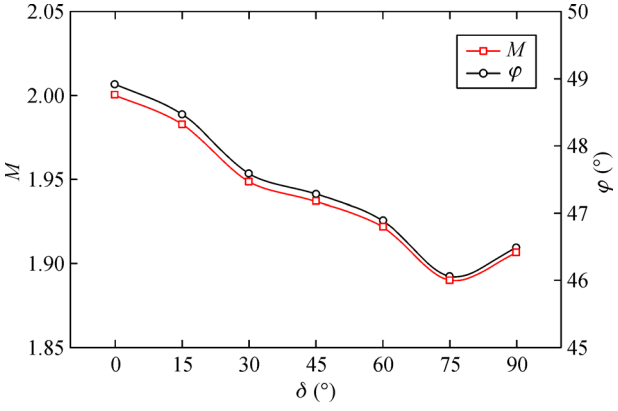


**Fig. 10** Shear strength in CD triaxial tests with various major principal stress direction angles.

Figure 11 illustrates the typical values of the volumetric strain of the specimens in the conventional CD triaxial tests

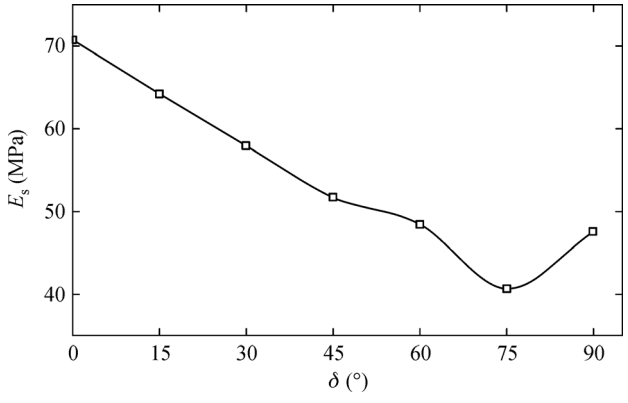


**Fig. 9** Initial secant modulus in CD triaxial tests with various major principal stress direction angles.

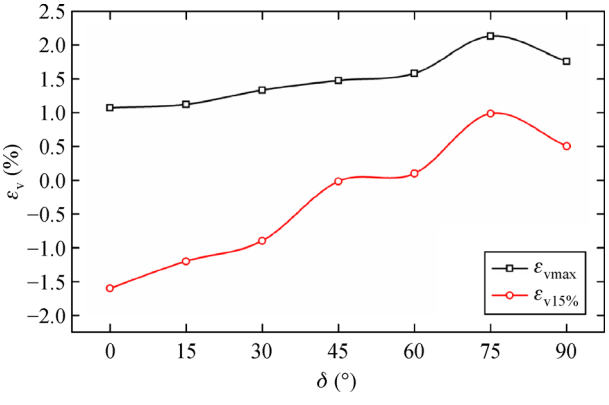


**Fig. 11** Volumetric strain in CD triaxial tests with various major principal stress direction angles.

with different major principal stress direction angles. The hollow square points denote the maximum volumetric strains of the specimens during the shear process, whereas the hollow dots represent the corresponding volumetric strains of the specimens at $\varepsilon_1$= 15%. According to Fig. 8(b) and Fig. 11, the maximum volumetric strain of the specimen increased gradually with an increase in $\delta$, and the corresponding axial strain of the specimen also increased until it reached its maximum value at $\delta$ = 75°. However, the maximum volumetric strain of the specimen decreased at $\delta$ = 90°. At $\varepsilon_1$ = 15%, the corresponding volumetric strain of the specimen exhibited obvious dilatancy. The maximum volumetric strain of the specimen was compression at $\delta$ = 75°, whereas it decreased slightly at $\delta$ = 90°.

## 4 Mechanism study on anisotropic mechanical properties of rockfill

Because rockfill is a type of granular material, the relative relationship between shear stress and normal stress can have a significant influence on the mechanical properties of the rockfill material. We define the plane of the maximum ratio of shear stress to normal stress in the specimens as the dominant shear plane, which corresponds to the straight line crossing the origin and the tangent points $A$ and $B$ on Mohr's stress circle. As shown in Fig. 12(a), the angle between the tangent line and the horizontal axis is called the dominant shear angle.

Figure 12(b) visualizes the relationship between the stress state, compaction plane, and dominant shear plane of the specimen. According to this and Fig. 12(a), the angle between the dominant shear plane and the major principal stress plane is clearly 45°+$\psi$/2, whereas the angle between the dominant shear plane and the compaction plane is 45°+$\psi$/2−$\delta$. Figure 12(b) also shows the relationship between the dominant shear plane and the main orientation of the particles at different positions. In the conventional triaxial test, with the increase in the axial stress (major principal stress), as shown in Fig. 12(a), the Mohr's stress circle enlarges to the right, such that $\psi$ increases. Consequently, the dominant shear plane becomes the failure plane. In this situation, the dominant shear angle is equal to the internal friction angle $\psi$.

Because the long axis of the particles tends to arrange along the compaction plane, the resistance to particle slippage in the compaction plane is relatively minimal. With respect to the rockfill material, the value of $\psi$ is usually approximately 50°; therefore, when $\delta$ is near 70°, the failure plane is parallel to the compaction plane, and the shear strength of the rockfill material should be at its lowest. This analysis agrees well with the test results.

To study the mechanism further, two cases with $\delta$ = 0° and $\delta$ = 75° were selected for a quantitative explanation. As shown in Figs. 13(a) and 13(b), when $\delta$ = 0°, the compaction plane C is parallel to the major principal stress plane H. At the start of the vertical loading or deviatoric stress, the angle between the compaction plane and the two dominant shear planes $A$ and $B$ is approximately 45°. As the deviatoric stress increases, this angle increases gradually, such that the corresponding interlocking resistance in planes $A$ and $B$ due to the particle orientation increases, and the dilatancy effect also increases. According to Fig. 8, the specimen, which has been undergoing contraction at this point, is then subjected to swelling at

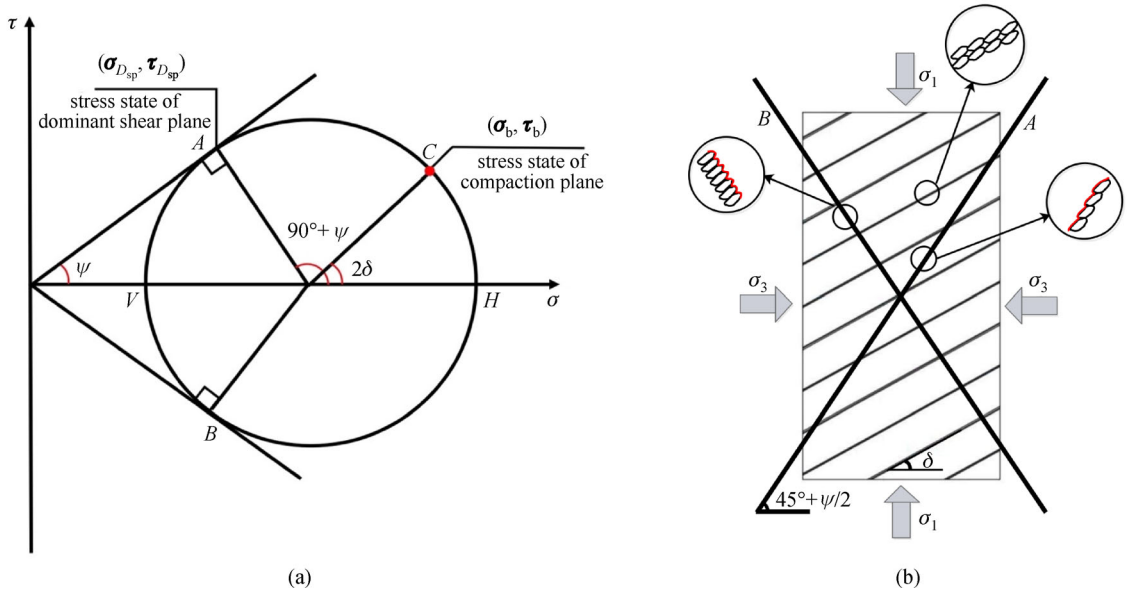


**Fig. 12** Schematic diagram of stress states on characteristic planes: (a) angles between characteristic planes in a Mohr's stresses circle; (b) relationship between the stress state, the compaction plane and the dominant shear plane of the specimen.

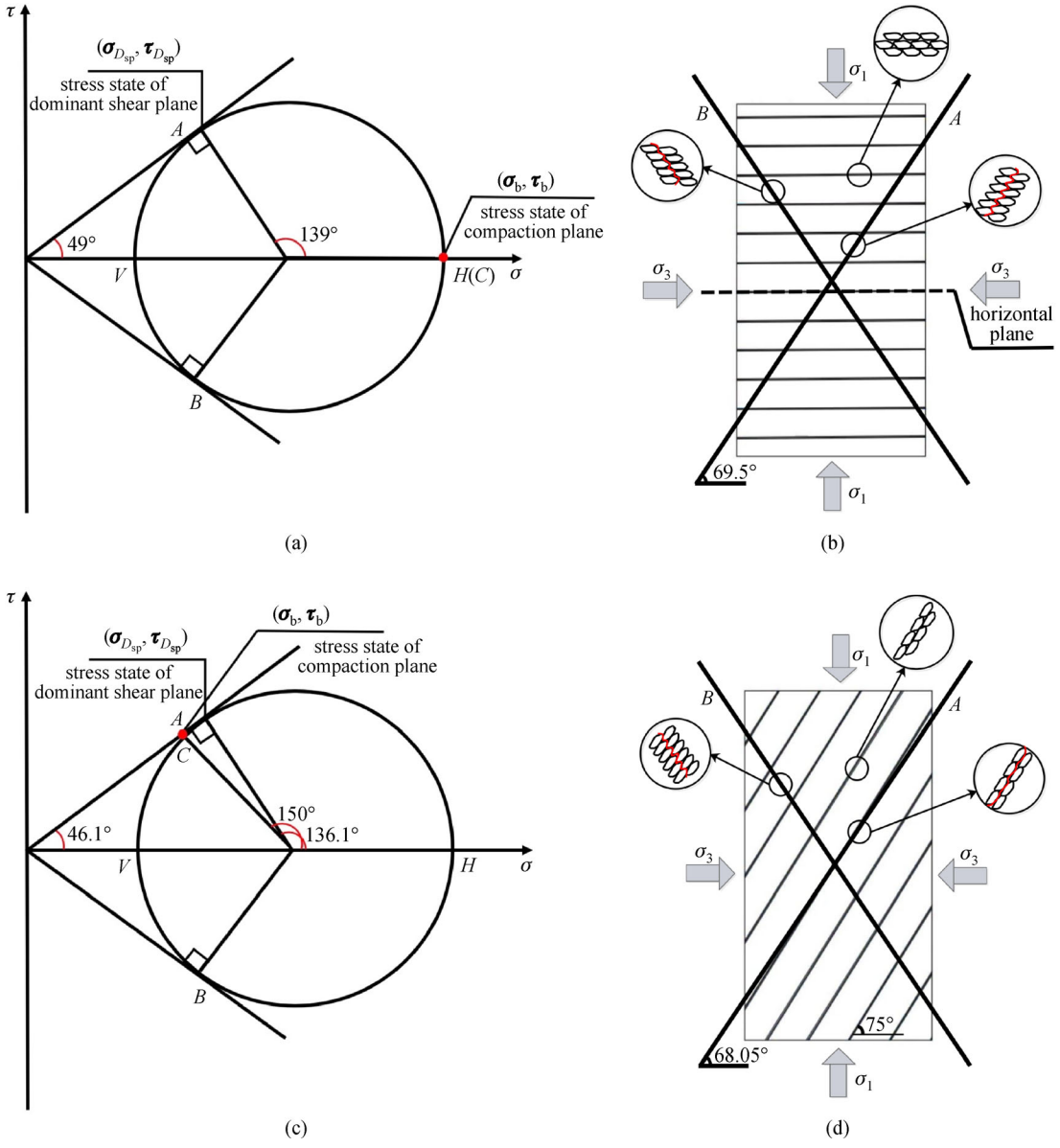


**Fig. 13** Schematic diagram of stress state at failure on characteristic plane for different major stress direction angles: (a) angles between characteristic planes in a Mohr's stresses circle ($\delta = 0°$); (b) relationship between the stress state, the compaction plane and the failure plane of the specimen ($\delta = 0°$); (c) angles between characteristic planes in a Mohr's stresses circle ($\delta = 75°$); (d) relationship between the stress state, the compaction plane and the failure plane of the specimen ($\delta = 75°$).

approximately 4% of the axial strain. When the axial strain reaches 15%, the angle between the compaction plane and the two dominant shear planes is approximately 69.5°. From Fig. 8, the amount of expansion is observed to be 1.5%, and a significant dilatancy remains.

As shown in Figs. 13(c) and 13(d), when $\delta$ is 75°, the angle between the compaction plane $C$ and the major principal stress plane $H$ is 75°. At the start of the vertical loading, the angles between the compaction plane and the two dominant shear planes $A$ and $B$ are approximately 30° and 60°, respectively. With the increase in deviatoric stress, the angles decrease gradually, such that the corresponding interlocking resistance in planes $A$ and $B$ due to the particle orientation decreases, and the dilatancy effect is also weakened. According to Fig. 8, the specimen, which has been undergoing contraction at this point, is then subjected to swelling at approximately 7.5% of the axial strain, which is significantly greater than the corresponding axial strain at $\delta = 0°$. When the axial strain of the specimen reaches 15%, the angles between the compaction plane and the two dominant shear planes $A$ and $B$ are approximately 6.9° and 36.9°, respectively, which are significantly smaller than those for $\delta = 0°$, especially when the dominant shear plane A is almost parallel to the compaction plane.

The interlocking resistance due to the particle orientation on this plane is clearly significantly reduced. According to Fig. 8, when the axial strain of the specimen is equal to 15%, although a tendency for dilatancy remains, the specimen undergoes contraction volumetric strain with respect to the initial state, with a magnitude of 1.0%.

A comprehensive analysis of the aforementioned results shows that the major principal stress direction angle has a significant effect on the mechanical properties of the rockfill material. The mechanism is that the angle between the compaction plane and the dominant shear plane is closely related to the interlocking resistance due to the particle orientation. Because this group of tests was conducted at a relatively low confining pressure of 400 kPa, all the tests with different $\delta$ demonstrated the tendency for dilatancy to some extent, with positive dilatancy following a negative one. This phenomenon results from the relatively high density of the rockfill specimen and the interlocking effect between particles. The direction of the compaction during specimen preparation changes the extent of the interlocking effect, which causes different angles of major principal stress to induce different anisotropies.

## 5 Conclusions

In this study, the geometric characteristics of a typical particle fraction, which consists of a certain rockfill material, were studied. To fulfil this objective, the particle orientation distributions in the specimens prepared using different compaction methods were statistically analyzed. A set of rockfill specimen preparation devices for inclined compaction planes was manufactured, such that a series of conventional triaxial compression tests, in which the major principal stress direction angles were different, could be conducted. Based on the relevant test results, the influence of the major principal stress direction angle on the mechanical properties of compacted rockfill materials was studied. The main conclusions are as follows.

1) The axial lengths of the rockfill material, which is characterized by large particle sizes, are clearly different in three different directions. The ratio of the maximum axial length to the minimum axial length is approximately 3 on average, whereas the maximum projected area is approximately 4 to 6 times that of the minimum.

2) For the low-density specimen, there are two peak values in the probability distribution histogram of the particle inclination angle. With the increase in compaction density, the peak value approaches zero, and thus the particle orientation tends to be horizontal. However, the probability distribution of the particle inclination angle of the high-density specimen has only one peak value, which is near 0° and relatively concentrated, indicating that intensive compaction in the specimen preparation process can significantly enhance the horizontal orientation of the particles.

3) A set of devices was manufactured for rockfill specimen preparation with different inclination angles of the compaction plane. The core component is a cubic mold box, which can be rotated at the bottom side, such that its inclination angle can be controlled by a retractable strut. Both the top and the side parallel to the rotating shaft can be opened and sealed with block-inserted baffles during layer-by-layer compaction. Sprinkling an appropriate amount of water on the surfaces of the specimens can enable them to be frozen evenly, such that the disturbance to the rockfill specimens can be effectively reduced during the specimen preparation and installation processes.

4) A series of conventional CD triaxial tests on compacted rockfill with different major principal stress direction angles was conducted. The tests revealed that the use of the manufactured specimen preparation device can effectively guarantee the density and shape of the rockfill specimen in the process of its preparation. Different specimen preparation tilting angles can lead to different compaction plane angles relative to the principal stress plane. As $\delta$ changes from small to large, both the shear strength (at 15% axial strain) and the initial tangent modulus of the rockfill specimen tend to change from decreasing to increasing. When the axial strains of specimens with different principal stress direction angles reach 15%, the stress–strain curves are clearly separated from each other. The maximum volumetric strain and volumetric strain at 15% axial strain of the rockfill specimen exhibit a change, from increasing to decreasing. The peak values of both volumetric strains occur at $\delta = 75°$.

5) Based on the relationship between the major principal stress direction angle, changes in the stress state, and change in the corresponding dominant shear plane, the influence of the major principal stress direction angle on the mechanical properties of the rockfill material was analyzed. The mechanism is that the angle between the compaction plane and the dominant shear plane is closely related to the interlocking resistance due to the orientation of the particles. Because this group of tests was conducted at a relatively low confining pressure of 400 kPa, all the tests with different $\delta$ demonstrate the tendency for dilatancy to some extent, with positive dilatancy following a negative one. This phenomenon results from the relatively high density of the rockfill specimen and the interlocking effect between the particles. The direction of the compaction during specimen preparation changes the extent of the interlocking effect, which causes different angles of major principal stress to induce different anisotropies.

**Acknowledgements** This work was supported by the National Key R&D Program of China (No. 2017YFC0404802) and the National Natural Science Foundation of China (Grant Nos. U1965206 and 51979143).

## References


1. Yin Z Z, Zhang K Y, Zhu J G. Anisotropy of soil considered in stress and deformation calculation of plane rockfill dam. Chinese Journal of Hydraulic Engineering, 2004, 35(11): 22–26 (in Chinese)
2. Gurevich B, Pervukhina M, Makarynska D. An analytic model for the stress-induced anisotropy of dry rocks. Geophysics, 2011, 76(3): WA125–WA133
3. Yang J, Li G Y, Shen T. Stress-deformation properties of super-high CFRDs under complex terrain conditions. Chinese Journal of Geotechnical Engineering, 2014, 23(4): 407–411 (in Chinese)
4. Jia Y A. Comparison and verification of constitutive models for rockfill materials under complex stress path. Dissertation for the Doctoral Degree. Beijing: Tsinghua University, 2006 (in Chinese)
5. Li X S, Dafalias Y F. Constitutive modeling of inherently anisotropic sand behavior. Journal of Geotechnical and Geoenvironmental Engineering, 2002, 128(10): 868–880
6. Shi W C. True triaxial test on coarse-grained soil and study on constitutive model. Dissertation for the Doctoral Degree. Nanjing: Hohai University, 2008 (in Chinese)
7. Wang Y, Yu Y Z, Wu Y K, Zhang B Y, Lv H, Sun X. Development and application of a large-scale static and dynamic true triaxial apparatus for gravel. International Journal of Geomechanics, 2018, 18(3): 04018004
8. Veiskarami M, Ghorbani A, Alavipour M. Development of a constitutive model for rockfills and similar granular materials based on the disturbed state concept. Frontiers of Structural and Civil Engineering, 2012, 6(4): 365–378
9. Zhang F, Ye B, Ye G L. Unified description of sand behavior. Frontiers of Architecture and Civil Engineering in China, 2011, 5(2): 121–150
10. Zhang D M, Yin Z Y, Hicher P Y, Huang H W. Analysis of cement-treated clay behavior by micromechanical approach. Frontiers of Structural and Civil Engineering, 2013, 7(2): 137–153
11. Huang M S, Yao Y P, Yin Z Y, Liu E L, Lei H Y. An overview on elementary mechanical behaviors, constitutive modeling and failure criterion of soils. China Civil Engineering Journal, 2016, 49(7): 9–35 (in Chinese)
12. Duncan J M, Seed H B. Anisotropy and stress reorientation in clay. Journal of the Soil Mechanics and Foundations Division, 1966, 92(5): 21–50
13. Tong Z X, Zhou S P, Yao Y P, Shi G. An improved direct shear apparatus for shear strength of anisotropic sands and its primary application. Chinese Journal of Rock Mechanics and Engineering, 2012, 31(12): 2579–2580 (in Chinese)
14. Guo P J. Modified direct shear test for anisotropic strength of sand. Journal of Geotechnical and Geoenvironmental Engineering, 2008, 134(9): 1311–1318
15. Oda M, Koishikawa I, Higuchi T. Experimental study of anisotropic shear strength of sand by plane strain test. Soil and Foundation, 1978, 18(1): 25–38
16. Yamada Y, Ishihara K. Anisotropic deformation characteristics of sand under three dimensional stress conditions. Soil and Foundation, 1979, 19(2): 79–94
17. Abelev A V, Lade P V. Effects of cross anisotropy on three-dimensional behavior of sand. I: Stress-strain behavior and shear banding. Journal of Engineering Mechanics, 2003, 129(2): 160–166
18. Lade P V, Abelev A V. Effects of cross anisotropy on three-dimensional behavior of sand. II: Volume change behavior and failure. Journal of Engineering Mechanics, 2003, 129(2): 167–174
19. Shao S J, Xu P, Wang Q, Dai Y F. True triaxial tests on anisotropic strength characteristics of loess. Chinese Journal of Geotechnical Engineering, 2014, 36(9): 1614–1623 (in Chinese)
20. Guo Y, Mo Y B. Research on inherent anisotropy of saturated sand specimen. Journal of Disaster Prevention and Mitigation Engineering, 2018, 38(02): 251–257 (in Chinese)
21. Wei K M, Zhu S. A generalized plasticity model to predict behaviors of the concrete-faced rock-fill dam under complex loading conditions. European Journal of Environmental and Civil Engineering, 2013, 17(7): 579–597
22. Symes M J, Gens A, Hight D W. Undrained anisotropy and principal stress rotation in saturated sand. Geotechnique, 1984, 34(1): 11–27
23. Sun Y F, Shen Y. Constitutive model of granular soils using fractional-order plastic-flow rule. International Journal of Geomechanics, 2017, 17(8): 04017025
24. Tong Z X. Research on deformation behavior and constitutive model of sands under cyclic rotation of principal stress axes. Dissertation for the Doctoral Degree. Beijing: Tsinghua University, 2008 (in Chinese)
25. Yu Y L. Research on constitutive law and mathematical model of anisotropic sands under rotation of principal stress axes. Dissertation for the Doctoral Degree. Beijing: Tsinghua University, 2010 (in Chinese)
26. Rodriguez N M. Experimental study of 3D failure plane for cross-anisotropic sand deposits during stress rotation. Dissertation for the Doctoral Degree. Washington, D.C.: Catholic University of America, 2012
27. Yang Z X, Yang J, Wang L Z. Micro-scale modeling of anisotropy effects on undrained behavior of granular soils. Granular Matter, 2013, 15(5): 557–572
28. Yang L T. Experimental study of soil anisotropy using hollow cylinder testing. Dissertation for the Doctoral Degree. Nottingham: University of Nottingham, 2013
29. Yang Z X, Li X S, Ming H Y. Fabric anisotropy and undrained shear behavior of granular soil. Shenzhen Daxue Xuebao (Ligong Ban). Journal of Shenzhen University Science and Engineering, 2009, 26(2): 158–163 (in Chinese)
30. Chaudhary S K, Kuwano J, Hashimoto S, Hayano Y, Nakamura Y. Effects of initial fabric and shearing direction on cyclic deformation characteristics of sand. Soil and Foundation, 2002, 42(1): 147–157
31. Yang Z X, Li X S, Yang J. Quantifying and modelling fabric anisotropy of granular soils. Geotechnique, 2008, 58(4): 237–248
32. Suwal L P, Kuwano R. Statically and dynamically measured poisson's ratio of granular soils on triaxial laboratory specimens. Geotechnical Testing Journal, 2013, 36(4): 493–505
33. Zhao C B, Hobbs B E, Ord A. Fundamentals of Computational Geoscience: Numerical Methods and Algorithms. Berlin: Springer, 2009
34. Zhao C B. Physical and Chemical Dissolution Front Instability in Porous Media: Theoretical Analyses and Computational Simula-

tions. Berlin: Springer, 2014
35. Xu M, Hong J T, Song E X. DEM study on the effect of particle breakage on the macro-and micro-behavior of rockfill sheared along different stress paths. Computers and Geotechnics, 2017, 89: 113–127
36. Luo T, Li G, Ooie T, Chan A H C, Fu S J, Zou W L. DEM modelling of macro- and meso-mechanisms for rockfill materials. Engineering Journal of Wuhan University, 2018, 51(07): 607–612 (in Chinese)
37. Zhang D. Numerical analysis and constitutive simulation of anisotropic granular materials considering fabric evolution. Dissertation for the Doctoral Degree. Beijing: University of Science and Technology Beijing, 2017 (in Chinese)
38. Chu F Y, Zhu J G, Zhao Y H, He S B. An elastoplastic model for granular soil considering initial anisotropy. Journal of Central South University (Natural Science Edition), 2012, 5(43): 1914–1919
39. Zhang K Y, Wen D B, Ma Q H. Three-dimensional anisotropic revision and experimental verification of elliptic parabolic double yield surface elastoplastic model. Journal of Rock Mechanics and Engineering, 2013, 32(8): 1692–1700
40. Oda M, Nakayama H. Introduction of inherent anisotropy of soils in the yield function. Studies in Applied Mechanics, 1988, 20: 81–90
41. Oda M, Nemat-Nasser S, Konishi J. Stress-induced anisotropy in granular masses. Soil and Foundation, 1985, 25(3): 85–97
42. Wang Y. The Mechanical characteristics of rockfill materials under true triaxial stress conditions. Dissertation for the Doctoral Degree. Beijing: Tsinghua University, 2018 (in Chinese)
43. Dong T, Kong L, Zheng Y R, Yuan Q M, Liu W Z. Equivalent nonlinear model considering the anisotropy and the stress directionality of geomaterials. Journal of Rock Mechanics and Engineering, 2018, 37(2): 506–512 (in Chinese)
44. Dong T, Zheng Y R, Kong L, Zhe M. Strength criteria and slipping planes of anisotropic sand considering direction of major principal stress. Chinese Journal of Geotechnical Engineering, 2018, 40(4): 736–742 (in Chinese)
45. Arthur J, Menzies B K. Inherent anisotropy in a sand. Geotechnique, 1972, 22(1): 115–128